Acta Crystallographica Section B
**Structural Science**
ISSN 0108-7681

# X-ray diffuse scattering from HMTA: analysis *via* a Monte Carlo model

**D. J. Goossens,[a,b]* A. P. Heerdegen[a] and T. R. Welberry[a]**

[a]Research School of Chemistry, The Australian National University, Canberra 0200, Australia, and [b]Department of Physics, The Australian National University, Canberra 0200, Australia

Correspondence e-mail: goossens@rsc.anu.edu.au

Received 25 September 2007
Accepted 17 April 2008

Hexamethylenetetramine (HMT, $C_6H_{12}N_4$, also referred to as urotropin) and azelaic acid [A, HOOC$-(CH_2)_7-$COOH] form a co-crystal or adduct (HMTA, also referred to as urotropin azelate) which exhibits several structural phases as a function of temperature. At room temperature, the structure is orthorhombic, but shows substantial disorder. Here, this disorder is explored by analyzing the diffuse scattering from single crystals of HMTA *via* Monte Carlo simulation. The disorder is in part occupational, with two orientations of azelaic acid occurring, and in part thermally induced, which is to say dynamic. The occupational disorder can be thought of as a combination of limited-range in-plane (*bc* plane) negative correlations combined with effectively zero correlation between planes (along **a**), rather like stacking faults. Size effect, the cross-correlation between molecular orientation and displacement from average position, is required to reproduce the observed diffuse scattering.

## 1. Introduction

Hexamethylenetetramine (HMT, $C_6H_{12}N_4$, also referred to as urotropin) and azelaic acid [A, HOOC$-(CH_2)_7-$COOH] have been shown to form a co-crystal or adduct (HMTA, also referred to as urotropin azelate) which exhibits several structural phases as a function of temperature (Bonin *et al.*, 2003; Hostettler *et al.*, 1999). At room temperature the system is orthorhombic with the space group *Bmmb* and lattice parameters $a$ = 9.416 (2), $b$ = 26.124 (5) and $c$ = 7.203 (1) Å (Bonin *et al.*, 2003). The structure is disordered and shows considerable diffuse scattering.

This study takes as its starting point the average structure from the literature (Bonin *et al.*, 2003). In the average structure the azelaic acid site is considered to be occupied by a superposition of two orientations of the azelaic acid molecule. To a good approximation the HMT can be considered as a rigid molecule whose only degrees of freedom are external, while the A may well be expected to show internal degrees of freedom, which is to say the molecule may need to be allowed to flex.

Fig. 1 shows the room-temperature structure of HMTA, where only one orientation of A has been shown for clarity.

An earlier, very comprehensive study of HMTA (Bonin *et al.*, 2003) discussed the diffuse scattering from HMTA and arrived at a correlation structure for molecular flips on A. The work presented here discusses a detailed analysis of the diffuse scattering, including a development of a three-dimensional Monte Carlo (MC) model of HMTA, which reproduces the key features observed in diffuse scattering

owing to both molecular flips *and* displacements. The model is then used to gain insight into the short-range structures present in the crystal.

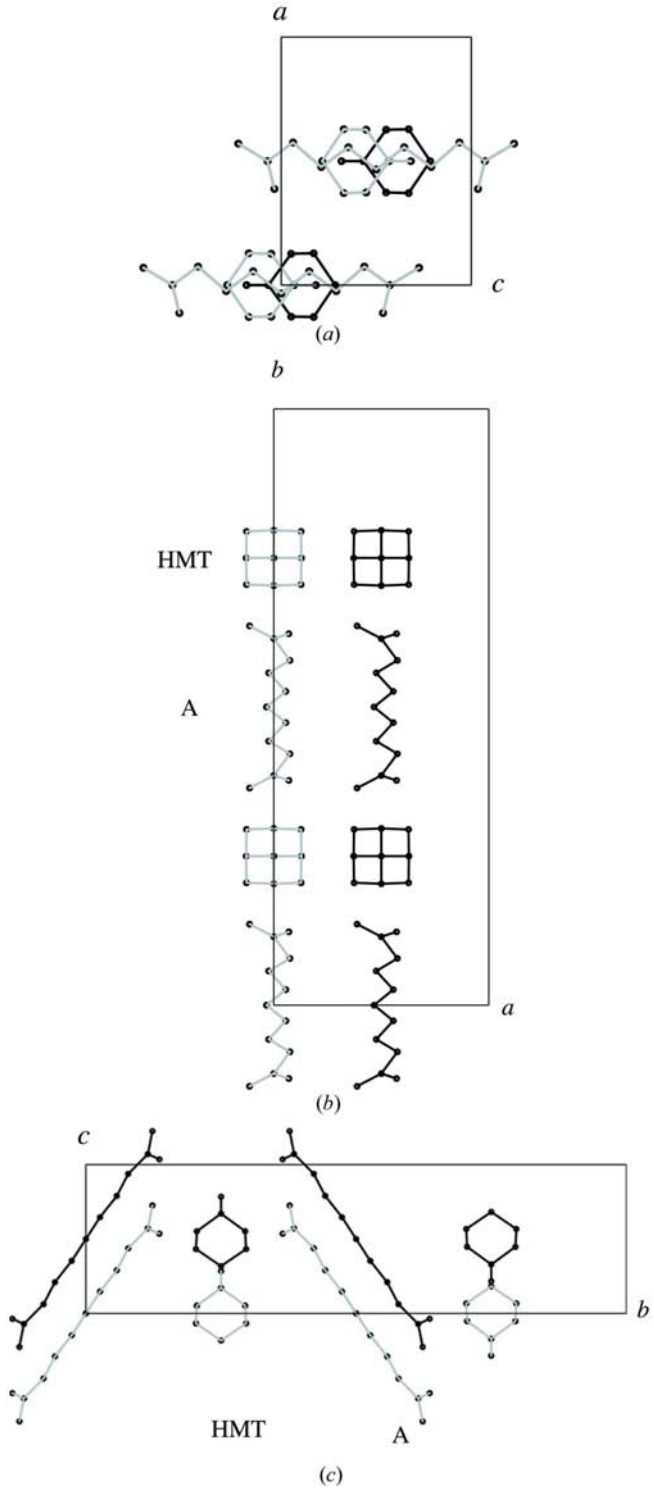


**Figure 1**
HMTA looking down the cell axes with a single orientation of azelaic acid molecule shown for clarity. H atoms are omitted. Boxes indicate the unit cell. Grey molecules are half a lattice parameter into (or out of) the page relative to the black. A more conventional representation of the structure can be found in Bonin *et al.* (2003).

## 2. Monte Carlo modelling

The MC model was implemented in Fortran90 running on Pentium 4 processors under Debian GNU/Linux. It follows the procedure set out previously (Welberry *et al.*, 2001; Goossens & Welberry, 2001) in that a $32 \times 32 \times 32$ unit cell 'crystal' is set up in the computer. Interactions between and within molecules are modelled in three ways:

(i) the energy associated with overall molecular orientations (in other words, occupational disorder) is given by an Ising-like term;

(ii) the energy associated with atomic or molecular displacements is modelled by harmonic springs between atoms;

(iii) potentials on bond angles, torsion angles and bond lengths give a molecular internal energy, allowing control of molecular flexibility.

For the modelling of overall molecular orientations the energy terms are essentially mechanisms for inducing the desired correlation structure. What structure is desired is determined interactively through comparisons with the occupancy features in the data. The force constants for the displacive and molecular internal energy and their relative scaling are determined empirically through comparison of the calculated diffraction patterns with the data.

### 2.1. Occupancies

The interaction of occupancies gives rise to an intermolecular energy. This was modelled first, with the resulting occupancy structure then fed into a simulation to allow the displacive disorder to be modelled. For HMTA only A shows occupational disorder, so only these molecules enter into the occupancy model. One orientation of A is essentially the 180° flip of the other about the long axis of the molecule. If $S = +1$ is allocated to one orientation and $S = -1$ to the other, the energy associated with the orientations (occupancies) can be modelled using an Ising-like term of the form

$$E_{\rm occ} = \sum_{\rm ov} \sum_{\rm pairs} F_{\rm ov} S_a S_b, \qquad (1)$$

where ov indicates occupancy vector types (nearest and second-nearest neighbours along all three directions were considered, but it was found that it was necessary to consider nearest neighbours in the *bc* plane only). The sum is over all pairs in the crystal separated by each type of vector. $F_{\rm ov}$ is the force constant associated with the vector ov. Hence by changing the sign of $F_{\rm ov}$ positive or negative correlations amongst the A orientations can be induced; the relative magnitudes of $F_{\rm ov}$ scale the correlations relative to each other while the absolute magnitudes relative to $k_B T$ govern the sizes of the correlations, subject to any frustration. $S_i$ is the occupancy variable, $\pm 1$, for site *i*.

In practice, a single MC step consists of randomly selecting a molecule and calculating its energy [see equation (1)], then randomly selecting another molecule of opposite occupancy and calculating its energy. The energy of the 'old' configuration ($E_{\rm old}$) is the sum of the energies of the two molecules. The occupancies are then exchanged and the energy calculations

repeated ($E_{\rm new}$). If energy is lower with occupancies exchanged ($E_{\rm new}<E_{\rm old}$), the new configuration is kept, otherwise the original configuration is retained, although at finite temperature there is some probability of accepting a move which increases energy. If when $E_{\rm new}>E_{\rm old}$

$$\exp\left(\frac{-(E_{\rm new}-E_{\rm old})}{k_BT}\right)>r, \qquad (2)$$

where $r$ is a random number from a uniform distribution 0 to 1, then the new configuration is incorporated into the model despite increasing the energy of the system.

If there is a total of $N_m$ molecules in the model, then a single MC cycle consists of $N_m$ such steps.

### 2.2. Displacements

To model correlations amongst displacements, the occupancy correlation structure is first established as discussed above, then displacements amongst the molecules are allowed to propagate *via* a set of intermolecular contact vectors. This set must be large enough to induce the features seen in the diffraction patterns, it must have symmetries such that the average structure is maintained, and the types of vectors must be limited enough to allow interpretation and modelling. Use is made of a set of 'effective' interactions between molecules.

The energy associated with a displacement is modelled using harmonic potentials. Thus, the total intermolecular energy associated with atomic and molecular displacements throughout the crystal is given by

$$E_{\rm disp}=\sum_{\rm cv}F_{\rm cv}(d_{\rm cv}-d_{0\rm cv})^2, \qquad (3)$$

where $d_{\rm cv}$ is the length of the vector, $d_{0\rm cv}$ is its equilibrium length and cv indexes the contact vector. The size effect – the influence of occupancy on preferred contact vector length – can be incorporated by allowing $d_{0\rm cv}$ to depend on the relative orientations of the interacting molecules. In this case, (3) is rewritten as

$$E_{\rm disp}=\sum_{\rm cv}F_{\rm cv}[d_{\rm cv}-(1+\varepsilon_{\pm\pm})d_{0\rm cv}]^2, \qquad (4)$$

where $\varepsilon_{\pm\pm}$ are the size-effect parameters. They obey the constraint

$$c_{--}\varepsilon_{--}+c_{-+}\varepsilon_{-+}+c_{+-}\varepsilon_{+-}+c_{++}\varepsilon_{++}=0, \qquad (5)$$

where $c_{\pm\pm}$ are the concentrations of the possible combinations of signs of occupancies, such that $\sum c_{\pm\pm}=1$.

The total intermolecular energy of the model crystal, $E_{\rm inter}$ is given by $E_{\rm inter}=E_{\rm occ}+E_{\rm disp}$. In practice, however, the occupancy simulation is done first, with the displacive simulation then operating on the 'static' occupancy structure.

### 2.3. Internal degrees of freedom

An extended molecule with many single bonds, like A, is expected to be able to flex. Hence, it is necessary to incorporate molecular flexibility into the modelling. Further, it may be reasonable to associate some energy penalty with this flexing. These degrees of freedom are built into the MC simulation by describing each molecule using a $z$-matrix. A $z$-matrix gives each atomic position relative to a local set of coordinates, in which the first atom–atom bond defines the (local) $z$ direction, the second defines $x$, and $y$ is chosen to complete a right-handed set of coordinates. Each atom is defined in terms of those defined previously, allowing a modification of an atom's position to be automatically manifested in the atoms dependent on it. The position of the origin atom and the orientation of the first bond are given in the crystal frame of reference by 'external' variables, a three-component vector, **x**, and a four-component vector (a quaternion), **q**, respectively.

Potentials can be put on these internal degrees of freedom if the flexing is thought to cost an energy penalty beyond that caused by the stretching or compressing of contact vectors [see (3)]. This results in an internal (*intra*molecular) energy, $E_{\rm intra}$. Not all internal degrees of freedom can be released – bond lengths can often be safely kept fixed, for example, while phenyl rings may be kept rigid while allowing them to librate. This was the case, for example, in fitting the diffuse scattering in molecules such as ibuprofen (Goossens, Heerdegen *et al.*, 2007; Altin & Goossens, 2007) and benzil, and its derivatives (Welberry *et al.*, 2001; Welberry & Heerdegen, 2003; Goossens *et al.*, 2005; Goossens, Welberry *et al.*, 2007).

During the displacement/internal variables simulation, the energy of a molecule is given by $E_{\rm intra}+E_{\rm disp}$, with the occupancies having an indirect effect through any size effect built into the model.

Considering the torsional degrees of freedom, the intramolecular energy can then be written

$$E_{\rm intra}=\sum_{{\rm mol},m}\sum_{i}F_i(\Delta\varphi_{im})^2+ +\sum_{ij}F_{ij}(\Delta\varphi_{im}\Delta\varphi_{jm}), \qquad (6)$$

where $i$ (or $j$) indexes the degrees of freedom within a molecule and the sum is over all molecules, $m$, with internal degrees of freedom, which in this case are the azelaic acid molecules (mol = molecules). $F$ is the torsional spring constant and $\Delta\phi$ is the deviation from the equilibrium position. Since it is possible for a twist on one torsion to in some sense 'compensate' for that on another, internal degrees of freedom are allowed to interact pairwise through cross terms of the form $F_{ij}(\Delta\varphi_{im}\Delta\varphi_{jm})$. The 'compensation' here means that it may be that if one torsion twists one way and another twists another way, then the twists may compensate for each other in that some atoms may not be shifted much despite the new conformation. This will act to make the two torsion angles interdependent (correlated in other words) and this energy term is one way to model this.

## 3. Experimental

Data were collected using a curved position-sensitive detector (PSD) system (Osborn & Welberry, 1990) from a single crystal of HMTA. Reciprocal space planes 0$kl$, 1$kl$, 2$kl$ and 3$kl$ were

collected and are reproduced in Fig. 2. The instrument collects two-dimensional cuts of data. In this case, cuts of constant $h$. By collecting several cuts at different values of $h$, a three-dimensional dataset is obtained. The data along one axis is less detailed than along the others. However, earlier results (Bonin *et al.*, 2003) from cuts in other directions have already shown that the key occupancy behaviour occurs in the real-space $bc$ plane, so cuts parallel with this plane are ideal.

Fig. 2 shows much prominent and complex diffuse scattering, particularly in the $h \neq 0$ layers. Some deductions can be made based on general principles used in the interpretation of diffuse scattering (Welberry, 2004). Since the 0$kl$ layer is descriptive of the structure when averaged along $a$, it shows no evidence of the occupancy effects. The presence of the diagonal streaks through the Bragg peaks (an example is indicated by arrow 'A') suggests that the displacive motions of the molecules are most strongly correlated along directions perpendicular to the streak direction, which is the direction of the backbone of the azelaic acid molecules when projected into the $bc$ plane. Some of the many strong diffuse spots when $h \neq 0$ (for example 'D' and 'E') *are* occupancy related and are suggestive of the onset of a superlattice owing to the alternating orientations of the azelaic acid molecules. The streaks through Bragg spots – apparent in these layers as well as 0$kl$ ('B', 'C') – are indicative of displacement correlations. The difference in the intensities of the two spots in box 'D' (there *is* a very weak spot at the right-hand end of the box) is greater than can be explained by scattering factor fall off.

The occupancy spots are much weaker but much broader in reciprocal space than the Bragg spots (the lower-most of the three Bragg spots in box 'B' in Fig. 2 shows as a single white pixel and indicates the limit of instrumental resolution at this level of data binning), indicating that instrumental resolution is not responsible for diffuse spot size and hence should not affect the estimation of occupancy correlation strengths and ranges.

While some of the displacive streaks are quite narrow in one direction (see box 'B' again), the measurement resolution is still easily good enough to show the strong anisotropy in these features, and little information appears to be lost.

The powder rings and considerable background intensity result from the sample degrading in the beam. They reduce the ability to analyse the data quantitatively.

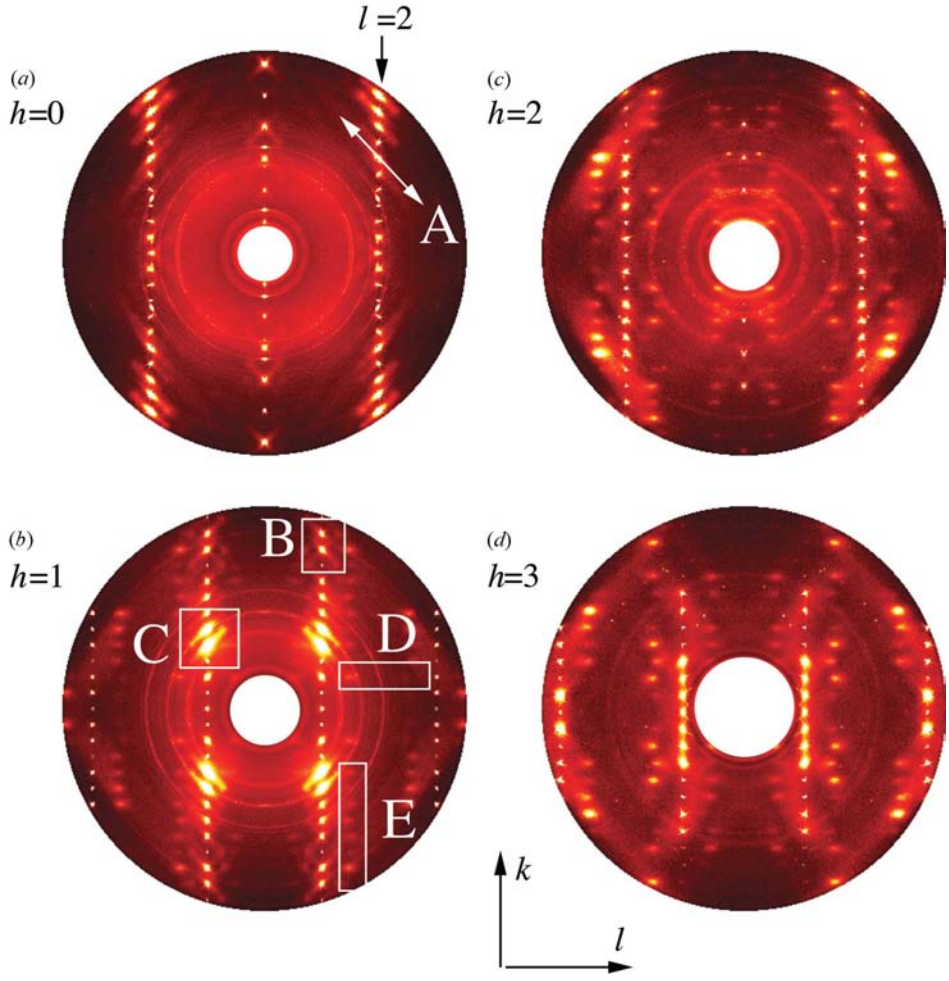


**Figure 2**
Cuts through reciprocal space for HMTA. (*a*) 0$kl$, (*b*) 1$kl$, (*c*) 2$kl$ and (*d*) 3$kl$. Letters A–E denote features discussed in the text.

## 4. Model crystal

### 4.1. *z*-matrices

The model crystal used in the MC was based on that from average crystal structures from the literature (Bonin *et al.*, 2003; Hostettler *et al.*, 1999) by describing the HMT and azelaic acid (A) using *z*-matrices. HMT and A occur four times in each unit cell and so the contents of the unit cell could be described using three *z*-matrices (one for HMT, one for each of the orientations of A), each accompanied by four **x** and four **q**. The diffuse scattering from the generated models was calculated using *DIFFUSE* (Butler & Welberry, 1992).

Table 1 shows the *z*-matrices used. Table 1(*a*) shows the HMT *z*-matrix, and Table 1(*b*) shows that of one orientation of azelaic acid; for the other the signs of the dihedral angles are reversed.

The model crystal consisted of $32 \times 32 \times 32$ unit cells with periodic boundary conditions.

**Table 1**
The *z*-matrices used in the *DIFFUSE* calculation.

(*a*) shows the HMT *z*-matrix, (*b*) shows azelaic acid in one orientation; reversing the signs of the dihedral angles gives the other. The resulting molecules are illustrated in Fig. 3.

| Number | Label | *l* | Distance from *l* (Å) | *m* | Angle with *lm* (°) | *n* | Dihedral angle with *lmn* (°) |
|---|---|---|---|---|---|---|---|
| (*a*) | | | | | | | |
| 1 | N1 | 0 | 0.000 | 0 | 0.000 | 0 | 0.000 |
| 2 | C7 | 1 | 1.472 | 0 | 0.000 | 0 | 0.000 |
| 3 | N2 | 2 | 1.446 | 1 | 112.303 | 0 | 0.000 |
| 4 | C8 | 3 | 1.460 | 2 | 108.692 | 1 | −57.890 |
| 5 | C9 | 1 | 1.467 | 2 | 107.791 | 3 | −59.380 |
| 6 | N1 | 5 | 1.467 | 1 | 111.255 | 2 | 58.319 |
| 7 | C7 | 6 | 1.472 | 5 | 107.788 | 1 | 58.326 |
| 8 | N2 | 7 | 1.446 | 6 | 112.303 | 5 | −59.382 |
| 9 | C7 | 6 | 1.472 | 7 | 108.257 | 5 | 116.338 |
| 10 | C7 | 8 | 1.446 | 7 | 107.608 | 4 | 117.539 |
| (*b*) | | | | | | | |
| 1 | C5 | 0 | 0.000 | 0 | 0.000 | 0 | 0.000 |
| 2 | C4 | 1 | 1.517 | 0 | 0.000 | 0 | 0.000 |
| 3 | C3 | 2 | 1.509 | 1 | 116.233 | 0 | 0.000 |
| 4 | C2 | 3 | 1.516 | 2 | 111.755 | 1 | −175.720 |
| 5 | C1 | 4 | 1.528 | 3 | 112.815 | 2 | −173.669 |
| 6 | O1 | 5 | 1.367 | 4 | 107.709 | 3 | −162.223 |
| 7 | O2 | 5 | 1.099 | 4 | 120.377 | 3 | 41.593 |
| 8 | C4*b* | 1 | 1.517 | 2 | 112.354 | 3 | −174.743 |
| 9 | C3*b* | 8 | 1.509 | 1 | 116.233 | 2 | −174.743 |
| 10 | C2*b* | 9 | 1.516 | 8 | 111.755 | 1 | −175.720 |
| 11 | C1*b* | 10 | 1.528 | 9 | 112.815 | 8 | −173.669 |
| 12 | O1*b* | 11 | 1.367 | 10 | 107.709 | 9 | −162.223 |
| 13 | O2*b* | 11 | 1.099 | 10 | 120.377 | 9 | 41.593 |

### 4.2. Contact vectors

The contact vectors, which are a subset of all the possible atom–atom vectors, can be classified in a number of ways. Table 2 lists and classifies them according to which molecules they connect. Hence there are three types of vectors: A–A, HMT–HMT and A–HMT. Vectors are grouped into sets; for example, the vectors with force constants $F_{1a}$, $F_{1b}$ and $F_{1c}$ are considered to form set 1. The vectors within a set substitute for each other depending on the occupancies; in effect, the $\varepsilon_{\pm\pm}$ in (4) are implemented by using several 'different' vectors, rather than a single vector with a modification of its length. The initial estimates for the lengths of these originate from the average structure, and the size effect is then applied.

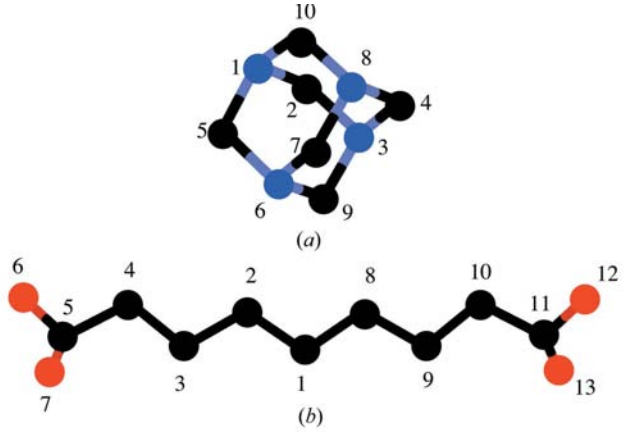


**Figure 3**
Molecules generated by the *z*-matrices in Table 1: (*a*) hexamethylenetetramine; (*b*) azelaic acid. Atom numbers give the corresponding row number in the *z*-matrix. Hence, for example, atom 1 in azelaic acid is C5, while for hexamethylenetetramine it is N1.

## 5. Modelling

### 5.1. Occupancies

Rods of scattering in Fig. 6 of Bonin *et al.* (2003) show that the occupancies are essentially uncorrelated along **a**. Spots in boxes 'D' and 'E' in Fig. 2 are cross sections through these rods and, in agreement with Bonin *et al.* (2003), they are not present in 0*kl*.

Fig. 4 shows diffuse scattering calculated from a model in which no displacements were allowed, but in which the orientations of the A molecules were correlated in the *bc* plane with nearest neighbours in both the *b* and *c* directions having a correlation of −0.5, which is to say nearest neighbours tend towards opposite occupancies, inducing a superlattice doubling along both axes. This gives rise to the rows of spots which can be seen to compare favourably with the diffuse spots present either side of the rows of Bragg peaks in Fig. 2(*b*). Only one layer is reproduced since the lack of *a*-axis correlations means that the occupancy spots in 2*kl* and 3*kl* are the same as those in 1*kl* (except for the X-ray form factor fall off). No spots show in the 0*kl* layer because it is the result of projecting all the molecules onto the basal plane, in which case

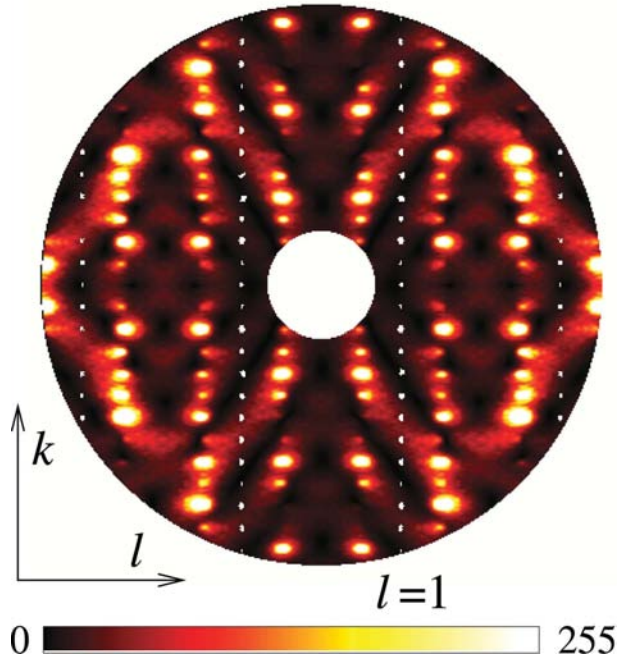


**Figure 4**
Calculated 1*kl* plane of reciprocal space, corresponding to Fig. 2(*b*), with no molecular displacements but with the nearest-neighbour *bc*-plane occupancy correlations set to −0.5. As with all calculated patterns, Bragg peaks have been ANDed with the image to provide a more direct comparison with the data. The bar below shows the colour map used.

**Table 2**
Contact vectors summarized.

A = azelaic acid, HMT = hexamethylenetetramine. 'Contact length' is the length from the *average* structure. Similar vectors which connect the same neighbours are grouped. Force constants are scaled such that the overall average $B$ factor is 6.0.

| Label | Contact length (Å) | Molecules connected | Model 2 force constant ($k_BT$, Å$^{-2}$) | Model 3 force constant ($k_BT$, Å$^{-2}$) | Model 3 size effect (Å) |
|---|---|---|---|---|---|
| $F_{1a}$ | 5.928 | A–A | 0.16 | 0.19 | 0.00 |
| $F_{1b}$ | 5.436 | A–A | 0.16 | 0.19 | 0.00 |
| $F_{1c}$ | 6.445 | A–A | 0.16 | 0.19 | 0.00 |
| $F_{2a}$ | 4.314 | A–A | 14.2 | 16.2 | 0.00 |
| $F_{2b}$ | 4.314 | A–A | 14.2 | 16.2 | 0.00 |
| $F_{3a}$ | 5.341 | A–A | 0.16 | 0.19 | 0.00 |
| $F_{3b}$ | 5.875 | A–A | 0.16 | 0.19 | 0.00 |
| $F_{3c}$ | 5.341 | A–A | 0.16 | 0.19 | 0.00 |
| $F_{4a}$ | 5.928 | A–A | 0.16 | 0.19 | 0.00 |
| $F_{4b}$ | 5.928 | A–A | 0.16 | 0.19 | 0.00 |
| $F_{4c}$ | 5.928 | A–A | 0.16 | 0.19 | 0.00 |
| $F_{5a}$ | 3.886 | A–A | 1.42 | 1.62 | −0.35 |
| $F_{5b}$ | 4.859 | A–A | 1.42 | 1.62 | 0.35 |
| $F_{5c}$ | 4.780 | A–A | 1.42 | 1.62 | 0.35 |
| $F_{5d}$ | 6.047 | A–A | 1.42 | 1.62 | −0.35 |
| $F_{6}$ | 3.843 | HMT–HMT | 0.09 | 0.11 | 0.00 |
| $F_{7}$ | 4.168 | HMT–HMT | 7.1 | 8.1 | 0.00 |
| $F_{8}$ | 4.285 | HMT–HMT | 0.09 | 0.11 | 0.00 |
| $F_{9}$ | 4.714 | HMT–HMT | 0.09 | 0.11 | 0.00 |
| $F_{10a}$ | 3.241 | A–HMT | 0.09 | 0.11 | 0.00 |
| $F_{10b}$ | 3.241 | A–HMT | 0.09 | 0.11 | 0.00 |
| $F_{11a}$ | 3.756 | A–HMT | 7.1 | 8.1 | 0.00 |
| $F_{11b}$ | 3.756 | A–HMT | 7.1 | 8.1 | 0.00 |
| $F_{12a}$ | 3.277 | A–HMT | 0.09 | 0.11 | 0.00 |
| $F_{12b}$ | 3.277 | A–HMT | 0.09 | 0.11 | 0.00 |
| $F_{13a}$ | 4.195 | A–HMT | 7.1 | 8.1 | 0.00 |
| $F_{13b}$ | 4.195 | A–HMT | 7.1 | 8.1 | 0.00 |
| $F_{14a}$ | 3.769 | A–HMT | 7.1 | 8.1 | 0.00 |
| $F_{14b}$ | 3.769 | A–HMT | 7.1 | 8.1 | 0.00 |
| $F_{15a}$ | 5.368 | A–HMT | 7.1 | 8.1 | 0.00 |
| $F_{15b}$ | 5.368 | A–HMT | 7.1 | 8.1 | 0.00 |

there are no 'occupancies' as each site has the average structure.

### 5.2. Displacements

Fig. 5 shows the first two layers calculated from a model ('Model 1') in which all the intermolecular $F_i$ are set to be equal and the model is forced to produce atomic displacement parameters such that the average $B_{iso}$ across all atoms is 6, which is approximately the value observed in Bragg refinements (Bonin *et al.*, 2003); this value contains a component due to the disorder and one due to the thermal motion of the atoms, which is appropriate as the simulation models both aspects of the structure.. The occupancies have nearest-neighbour *bc* plane correlations of −0.5 as for Fig. 4. All molecules are kept internally rigid. This simple model has induced a number of important features, such as the streaking around the Bragg peaks in the 0*kl* plane (although it is far too broad) and the four bright pairs of spots near the centre of the 1*kl* plane (box 'C' in Fig. 2). However, these spots should be far more elongated perpendicular to the radial direction, indicating the need for anisotropy in the displacive interactions.

The spots in Fig. 5(*b*) corresponding to those seen in Fig. 2 box 'D' are of very similar intensity, whereas the inner spot should be far brighter. This is also the case in Fig. 4(*b*), and suggests a need for some size effects to be introduced into the model (see below).

Inspection of Fig. 2 shows that there is streaking of the diffuse scattering in a direction transverse to a line approximately 45° to the $b^*$ ($k$) direction (streaking is noted by arrow 'A' in Fig. 2*a*). This indicates strong correlations along direc-

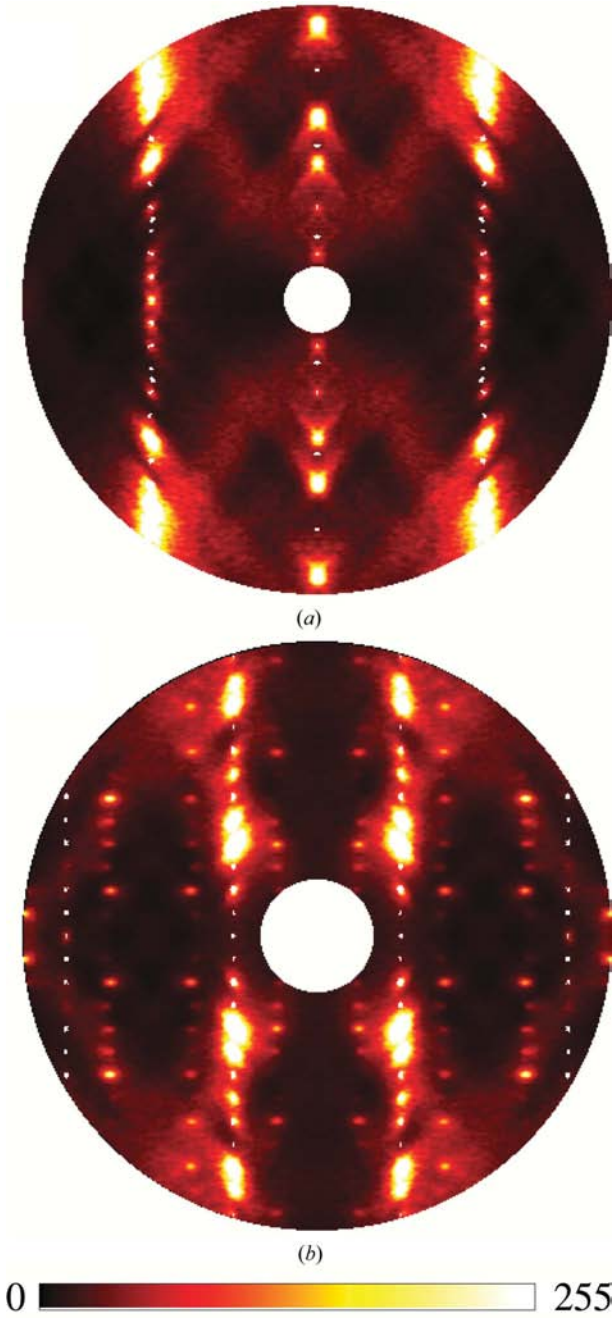


**Figure 5**
Calculated planes through reciprocal space corresponding to (*a*) and (*b*) in Fig. 2, with occupancies as for Fig. 4 and all spring constants set to be equal such that the average $B_{iso} = 6.0$. No size effect or internal degrees of freedom were applied. (*a*) 0*kl*; (*b*) 1*kl*.

tions $\sim 45^\circ$ to the $b$ axis. The contact vectors which have a projection substantially along this direction are classes 2, 7, 11 and 13–15. Of these, 7, 11 and 13 run parallel to the backbones of the associated A molecules, and the others are transverse. With these interactions enhanced by varying degrees determined interactively (see column 'Model 2' in Table 2), the diffraction patterns shown in Fig. 6 are obtained – with the elongation of the diffuse scattering agreeing quite well with that observed in the equivalent planes shown in Fig. 2. This is 'Model 2' in Table 2.

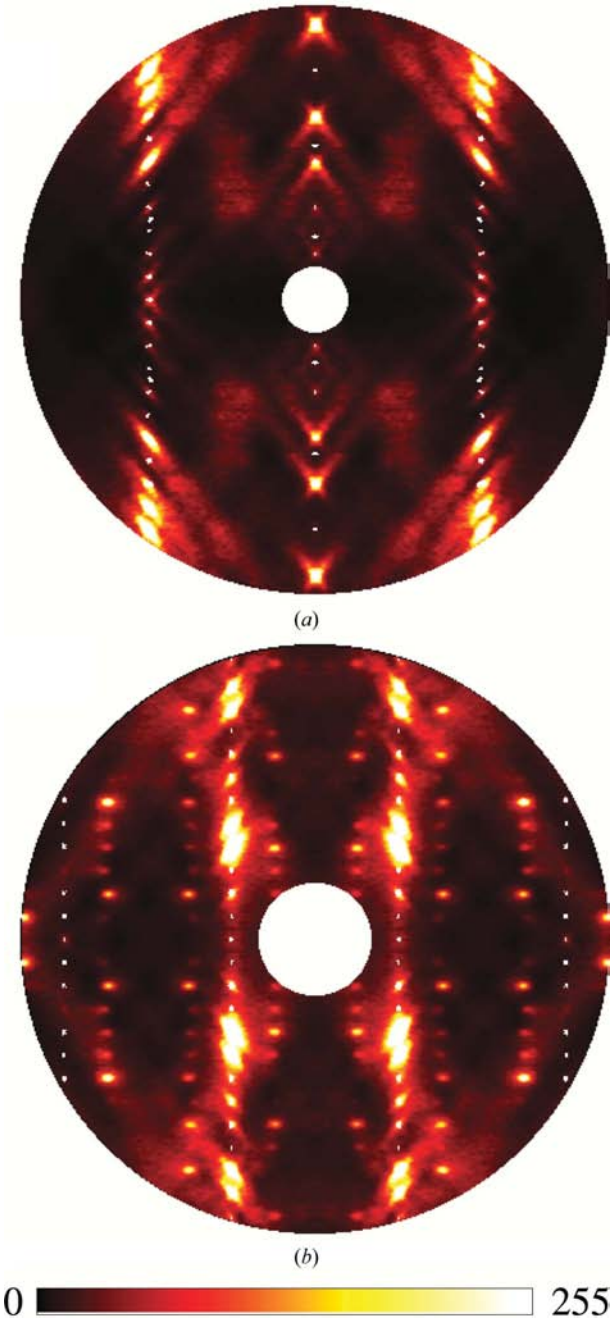


**Figure 6**
Calculated planes through reciprocal space corresponding to (*a*) and (*b*) in Fig. 2, with occupancies as for Fig. 4 and all spring constants roughly parallel to the directions $\sim \pm 45^\circ$ to the $b$ axis enhanced over the others ('Model 2' in Table 2); average $B_{iso} = 6.0$. No size effect or internal degrees of freedom were applied. (*a*) 0*kl*; (*b*) 1*kl*.

### 5.3. Size effect

Given the enormous number of degrees of freedom in the system – molecular occupancy, molecular displacement, the possibility of molecular flexibility and interactions between all these factors – determining a 'final' model is difficult. It becomes a compromise between excessive numbers of parameters and the quality of agreement with the data.

With this in mind, the application of size effect was explored. As one of the key indicators of size effect is the relative intensity of the two spots in box 'D' in Fig. 2, which is a transfer of intensity parallel to $c^*$, it was decided to look for contact vectors whose primary direction of propagation, when projected onto the *kl* plane, was the $c^*$ direction. From Fig. 1 it is apparent that such vectors will be A–A vectors, since the stacking –A–HMT–A–HMT– is along $b^*$. The set of vectors that best satisfies this criteria is set 5 (Table 2). This set consists of four vectors: 5*a* and 5*d* connect molecules of 'like' occupancy, while 5*b* and 5*c* connect those of unlike occupancy. This is illustrated in Fig. 7.

The diffraction patterns calculated from this model are shown in Fig. 8. It differs from model 2 only in that the size effects have been applied and the spring constants of the size-effected vectors have been increased.

Fig. 9 shows the *h*1*l* and *h*4*l* planes of reciprocal space calculated from model 3. Comparison with Fig. 6 from Bonin *et al.* (2003) shows that the model is quite good, with the streaks well captured and the thermal blobs also well reproduced.

Molecular flexibility was explored – for example the COOH groups of A were allowed to rotate. However, agreement between model and data was improved little relative to model 3. Given the added complexity of the model, these extra degrees of freedom could not be justified, so model 3 was considered the 'best' model.

## 6. Analysing the model

Once a satisfactory model has been established (model 3, Fig. 8), it can be explored. The assumption is that a model crystal which produces diffuse scattering patterns similar to those

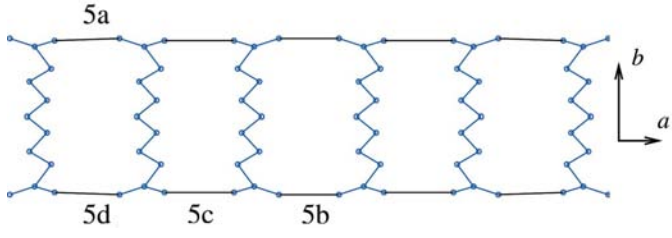


**Figure 7**
Contact vectors of set 5 in Table 2, the ones on which size effect is applied to generate the model whose diffraction patterns are shown in Fig. 8.

from the real crystal has similar short-range order (SRO) to that found in the real crystal.

Explorations of correlations among variables with a single molecule show that the $y$ and $z$ coordinates of an A molecule show a correlation of magnitude $\sim 0.3$. This is reasonable if it is allowed that the molecules are most likely to move along their length (see Fig. 1), which is a motion in the $bc$ plane. Of the 12 cross-correlations between the quaternion components and the coordinates of the molecular origin, nine are of magnitude less than 0.1 for A, with the strongest of these being that between the $y$ coordinate of the origin and $q_3$ (keeping in mind that the $q_i$ are not independent due to normalization of **q**) and having the value $\sim 0.2$. For HMT the strongest is that between the $z$ coordinate of the origin and $q_3$ and has the value $-0.58$, and only one of the cross-correlations has a magnitude *less* than 0.1.

When looking at correlations *between* A and HMT connected by the strong contacts that run at 45° in the $bc$ plane (Table 3) it can be seen that the $y_A - y_{HMT}$ and $z_A - z_{HMT}$ correlations are by far the most significant, followed by those between $z_A$ and some components of $\mathbf{q}_{HMT}$. This is in accordance with the strong correlations between **x** and **q** within HMT.

**Table 3**
Correlations between positions and orientations of HMT and A (connected by contact vectors of type 13) as revealed by X-ray diffuse scattering.

| | Azelaic acid | | | | | | |
|---|---|---|---|---|---|---|---|
| HMT | $x$ | $y$ | $z$ | $q_1$ | $q_2$ | $q_3$ | $q_4$ |
| $x$ | 0.17 | −0.03 | 0.00 | −0.04 | 0.01 | −0.06 | −0.05 |
| $y$ | 0.00 | 0.38 | −0.15 | 0.04 | 0.04 | −0.05 | −0.06 |
| $z$ | −0.01 | −0.27 | 0.51 | 0.06 | 0.06 | −0.01 | 0.01 |
| $q_1$ | 0.02 | 0.13 | −0.19 | −0.07 | −0.02 | −0.06 | −0.03 |
| $q_2$ | −0.04 | 0.14 | −0.22 | −0.02 | −0.10 | 0.03 | −0.05 |
| $q_3$ | 0.02 | 0.16 | −0.23 | 0.01 | −0.01 | 0.05 | 0.03 |
| $q_4$ | 0.06 | 0.12 | −0.14 | −0.04 | 0.05 | −0.04 | 0.03 |

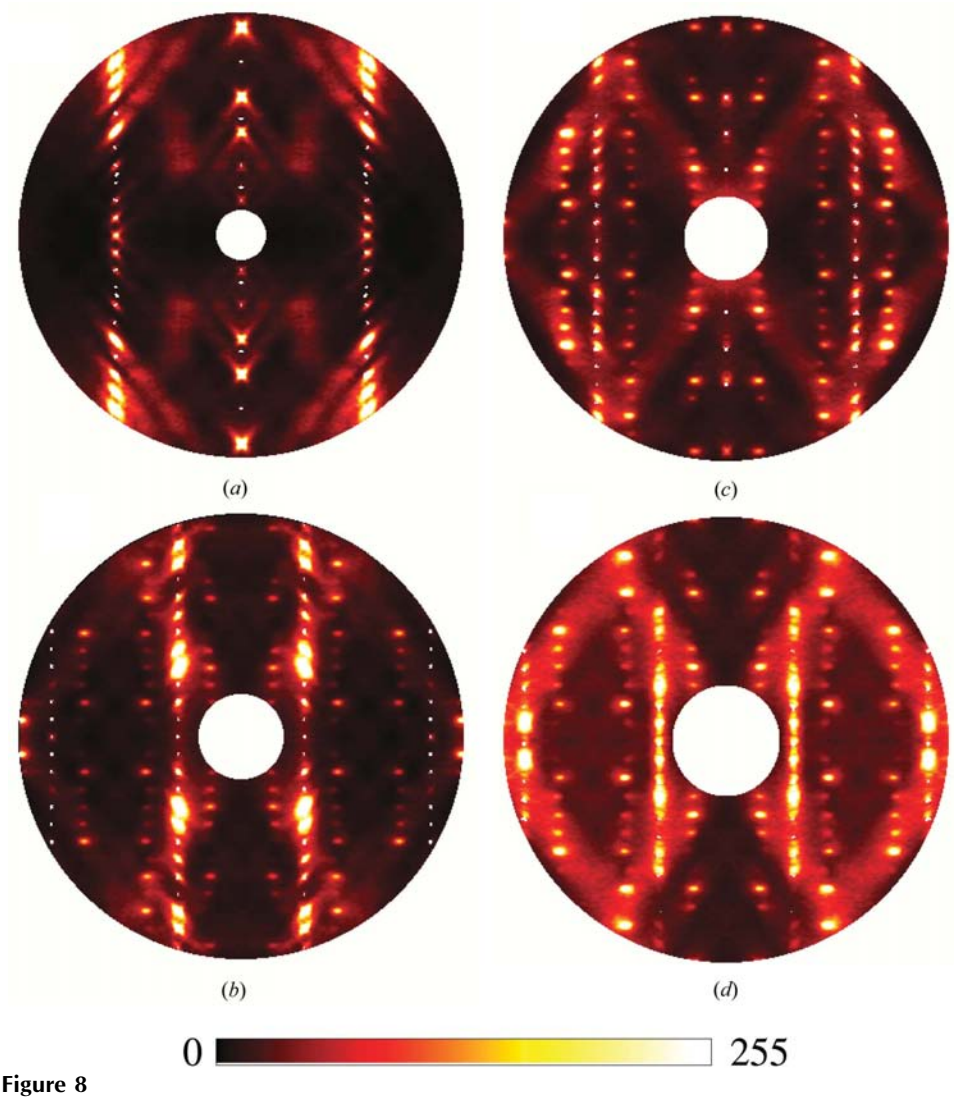


**Figure 8**
Calculated planes through reciprocal space corresponding to those in Fig. 2, with occupancies as for Fig. 4, spring constants as for 'Model 3' in Table 2 and size effects as noted in the 'size effect' column in Table 2. (*a*) 0*kl*; (*b*) 1*kl*; (*c*) 2*kl*; (*d*) 3*kl*.

Hence, the picture is one in which longitudinal $bc$ plane motions of A are transmitted (within the $bc$ plane) from A to A *via* the coupled rotation and displacement of the intervening HMT molecules. This information is presented graphically in Fig. 10, which shows the correlation between displacements on connected A and HMT molecules as a function of displacement direction; for example, Fig. 10(*a*) shows that displacements parallel to $b$ are much more highly correlated than those parallel to $a$, while in the $bc$ plane the displacements in all directions on the two molecules are quite highly correlated. This contact vector lies in the direction of the A backbone. The diagram shows A–HMT correlations; since these are the same as HMT–A, this leads to A–A correlations (for A molecules connect *via* the HMT layers) being the 'squares' of the A–HMT, so even the 'strong' correlations (*e.g.* $bc$ plane) will be relatively weak.

Fig. 11 plots histograms of the contact lengths for set 5 vectors from the final model crystal, with the equilibrium lengths subtracted. It shows that the vectors connecting 'like' orientations of A (5*a* and 5*d*) are on average shorter than the average, while others are longer. This reflects the ability of

the molecules to pack in the different configurations. While the size effects are of the order 0.35 Å, the actual distributions are centred within 0.14 Å of the 'un-size-effected' distance.

## 7. Conclusions

Based on the diffuse scattering data shown in Fig. 2, it appears that the A molecules in HMTA show substantial short-range orientational order in which adjacent molecules in *b* and *c* prefer to be of opposite orientation (correlations of −0.5 in both directions); given that the nearest neighbours in *b* are separated by HMT molecules, this implies that the HMTs are transmitting the interaction, something in which their inherent rigid cage shape will be crucial. This is reinforced by the displacive results, which show that there are substantial correlations between A and HMT variables within the *bc* planes.

Displacively, the strongest interactions were found to be in the diagonal directions within the *bc* plane, which is along the lengths of the A molecules, suggesting that the structure can be considered largely as a series of weakly interacting planes stacked up along *a*. This is in accordance with the occupancy structure, for which the best model was obtained with occupancies uncorrelated along *a*.

Size effect contributed to improving the balance of intensity of the spots in box 'D' of Fig. 2(*b*), but the ratio is still not extreme enough in the model. Synchrotron data may contain enough detailed information to determine the O-atom distri-

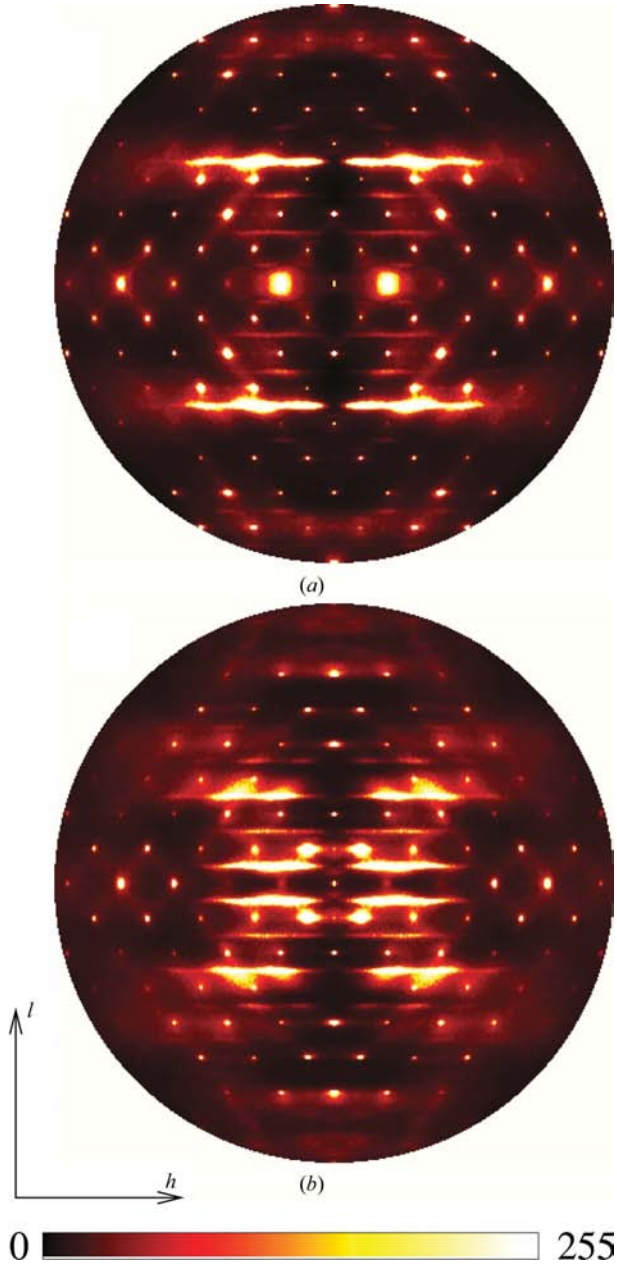


**Figure 9**
Calculated planes through reciprocal space from model 3, corresponding to those in Figs. 6(*a*) and (*b*) of Bonin *et al.* (2003). (*a*) *h*1*l*; (*b*) *h*4*l*.

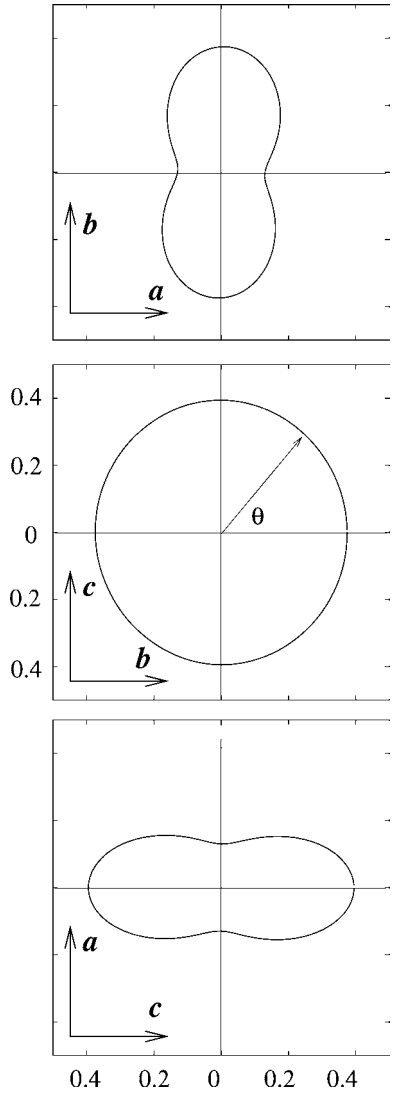


**Figure 10**
Correlations between molecular origin displacements on A and HMT molecules connected by contact vector 13*b*. $\theta$ is the angle the displacements make to the horizontal axis and the length of the arrow gives the size of the correlation.

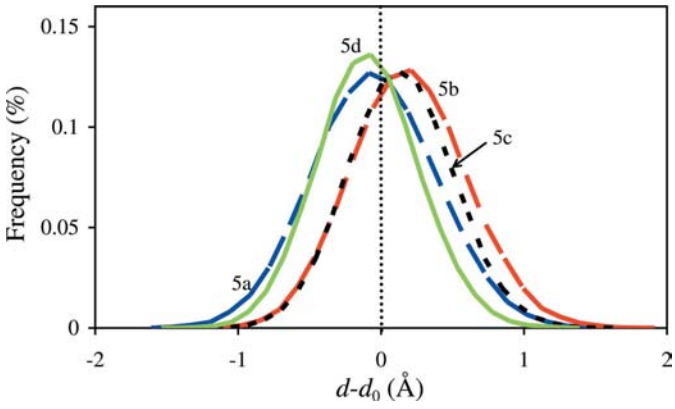


**Figure 11**
Histograms of the lengths of the type 5 contact vectors in the final model 3 simulation.

bution in more detail, although sample degradation could be a significant problem at such an intense source.

HMTA is a complex system; multiple types of molecules showing occupational and displacive disorder, combined with the potential for molecular flexibility *and* size effect result in a system with a great many possible forms of disorder and SRO. That it is possible to model the diffuse scattering at all, let alone with considerable agreement with experiment, and then analyse the model meaningfully is encouraging. The difficulties inherent in structure prediction of flexible molecular systems (Day *et al.*, 2005) show that the study of such systems is far from simple, and it is hoped that the analysis of diffuse scattering can begin to offer new insights into this important and diverse (and very common) class of molecular materials, including molecules of industrial and medical significance.

We acknowledge M. Gardon for providing a crystal. We acknowledge the Australian Partnership for Advanced Computing and the Australian Research Council for financial support. DJG gratefully acknowledges the support of the Australian Institute for Nuclear Science and Engineering.

## References

Altin, P. A. & Goossens, D. J. (2007). Proceedings-31st Annual Condensed Matter and Materials Meeting, http://www.aip.org.au/wagga2007/2007_2.pdf.
Bonin, M., Welberry, T. R., Hostettler, M., Gardon, M., Birkedal, H., Chapuis, G., Möckli, P., Ogle, C. A. & Schenk, K. J. (2003). *Acta Cryst.* B**59**, 72–86.
Butler, B. D. & Welberry, T. R. (1992). *J. Appl. Cryst.* **25**, 391–399.
Day, G. M. *et al.* (2005). *Acta Cryst.* B**61**, 511–527.
Goossens, D. J., Heerdegen, A. P., Welberry, T. R. & Beasley, A. G. (2007). *Int. J. Pharm.* **343**, 59–68.
Goossens, D. J. & Welberry, T. R. (2001). *Comput. Phys. Commun.* **142**, 387–390.
Goossens, D. J., Welberry, T. R., Heerdegen, A. P. & Edwards, A. J. (2005). *Z. Kristallogr.* **220**, 1035–1042.
Goossens, D. J., Welberry, T. R., Heerdegen, A. P. & Gutmann, M. J. (2007). *Acta Cryst.* A**63**, 30–35.
Hostettler, M., Birkedal, H., Gardon, M., Chapuis, G., Schwarzenbach, D. & Bonin, M. (1999). *Acta Cryst.* B**55**, 448–458.
Osborn, J. C. & Welberry, T. R. (1990). *J. Appl. Cryst.* **23**, 476–484.
Welberry, T. R. (2004). *Diffuse X-ray Scattering and Models of Disorder.* Oxford University Press.
Welberry, T. R., Goossens, D. J., Edwards, A. J. & David, W. I. F. (2001). *Acta Cryst.* A**57**, 101–109.
Welberry, T. R. & Heerdegen, A. P. (2003). *Acta Cryst.* B**59**, 760–769.